LAWRENCE
LIVERMORE
NATIONAL
LABORATORY

LLNL-JRNL-600673

Focused-ion-beam Assisted Growth, Patterning, and Narrowing the Size Sidtributions of ZnO Nanowires for Variable Optical Properties and Enhanced Non-mechanical Energy Conversion

X. Y. Wang, S. F. Xie, J. Liu, S. O. Kucheyev, Y. M. Wang

November 12, 2012

Chemistry of Materials

Disclaimer

Focused-ion-beam Assisted Growth, Patterning, and Narrowing the Size Distributions of ZnO Nanowires for Variable Optical Properties and Enhanced Non-mechanical Energy Conversion

Xianying Wang[†], Shufang Xie[†], Jian Liu[†], Sergei O. Kucheyev[‡], Y. Morris Wang[‡*]

[†]School of Materials Science and Engineering, University of Shanghai for Science and Technology, Shanghai, China, and [‡]Physical and Life Sciences Directorate, Lawrence Livermore National Laboratory, Livermore, CA, USA

ABSTRACT

Despite extensive research and much progress, it remains critical and challenging to precisely grow nanowires structurally and dimensionally uniform. Here we present a focused-ion-beam (FIB) assisted approach to controlling the ZnO nanowire growth with uniform diameters, height, and high crystalline quality. Vertical-alignment is also achieved on nonepitaxial substrates without the assistance of ZnO seeding layers (e.g., silicon and c-plane sapphire substrates). The programmable ability of FIB opens up new opportunities of creating complex patterns in our approach. A new alloy catalyst Au-Ga is developed for ZnO growth, with achievable narrow nanowire size distributions. Comparison studies of growth behavior in the temperature range of 880-940 ^{o}C for Au and Au-Ga catalysts reveal different growth kinetics and rate-controlling mechanisms that are consistent with the vertical-alignment and drastically improved nanowire uniformity for FIB-assisted nanowire growth. Nanogenerators built with improved nanowire platform exhibit a 2.5-fold increase in thermal energy conversion, demonstrating the promise of our approach for advanced functional devices.

KEYWORDS

ZnO nanowire; Au-Ga catalyst; focused-ion-beam; growth; activation energy; nanogenerator

*Contact email: ymwang@llnl.gov

▪ INTRODUCTION

The versatile, charismatic, ecofriendly, yet often capricious properties of ZnO nanostructures have spurred all-embracing research on these materials over the last decade,[1-4] with the morphology, size, and orientation control as one of the key measures in order to tailor their electronic or optical characteristics for various device applications.[5-7] In fact, ZnO has one of the most coveted varieties of morphologies reported to date (with more than a dozen of nanostructure shapes),[8-12] among which ordered arrays of one-dimensional (1-D) nanowires (NWs) have and will continue to play key roles as building blocks for existing and future optoelectronics,[13] nanogenerators,[14] solar cells,[2, 15] and sensors.[16] These vertically-aligned ZnO NWs sometimes also serve as templates for synthesizing other more exotic semiconductor nanostructures (e.g., nanotubes) and thus open up new opportunities for lithium-ion battery applications or for 3-dimentional (3-D) device integrations.[17, 18] A brief survey of the literature indicates that most NWs are overwhelmingly fabricated from two basic synthesis routes; i.e., liquid (solution) growth[6] and vapor growth.[3, 4] One of the later examples known as chemical vapor transport and condensation (CVTC) process is especially recognized for its simplicity and capability of producing high-crystallinity vertically-aligned NWs on various substrates.[13, 14, 19] However, the approach itself can be deceptively simple,[20] as a simple tweak of synthesis conditions (e.g., temperature, carrier gas, catalyst, or substrate) could lead to a vastly different mix of nanostructures with dissimilar electronic properties. Confusions further arise in terms of growth mechanisms, as both vapor-liquid-solid (VLS) and vapor-solid-solid (VSS) mechanisms are commonly invoked to rationalize growth (depending upon the types of nanostructures and growth conditions). As such, for 3-D device integrations reproducible synthesis of ZnO NWs with designated patterns, positions, spacing, alignments, densities, aspect ratios, and desired physical properties remains critical and is an area of active research.[6, 21] The size, position, and height-uniformity control is expected to become even more pressing when these ordered ZnO NWs act as templates for other more advanced semiconductor nanostructures.[17, 18]

For a typical CVTC synthesis of vertically-aligned ZnO NWs,[3, 22, 23] a thin Au film catalyst on a silicon or single-crystal sapphire (Al_2O_3) substrate is widely used. While this process is adequate to produce high-quality single crystalline NWs, it lacks the control of NWs density, diameter, and height uniformity due to the randomness of the film breakup at synthesis temperatures. In addition, the high degree of vertical-alignment is conventionally achieved for ZnO NWs grown epitaxially on a-plane Al_2O_3 or GaN substrate,[13, 14] whereas it is considered nontrivial for nonepitaxial substrates (e.g., silicon, c-plane Al_2O_3, and others) unless with the assistance of textured ZnO seeding layers.[8, 22] Approaches using gold nanoparticles[24] help position, diameter and density control, but encounter difficulty in tailoring height uniformity. More advanced techniques such as laser interference lithography may offer large scale and more uniform NWs in terms of height and diameter;[7] but the lateral dimensions of these NWs are generally large (in the submicron regime), which to some extent limits the tunable electronic or optical properties and the device fabrications.

In this work, we present a simplistic but very effective approach to help control ZnO NWs diameter-distribution and height-uniformity, together with programmable positioning capability. As illustrated in Fig. 1A, our approach relies on the delicate Ga+ ion implantation ability of the focused-ion-beam (FIB) technique. This approach is counterintuitive as such implantation effect is historically considered deleterious or undesirable. Previously, FIB has been applied to pinpoint the catalyst deposition location and help to grow 3-D Si NW branches, the principle of which is fundamentally different from our approach.[25] In our protocol NW growth experiments, Au thin film is deposited on an a- or c-plane Al_2O_3 substrate; the desired NWs growth area is exposed to low current Ga+ ion beam with an incident angle of 90^o for a short period of time, after which conventional CVTC growth is conducted (see *Materials and Methods*). We find that high-density ZnO NWs with very narrow diameter distributions and nearly uniform length are obtained in Ga^+ beam treated area, together with much higher growth rate. Conversely, Au catalyst can be completely bombarded off by FIB with larger beam currents and/or longer etching time, the area of which will have no NWs growth; i.e., our method can readily register

(either negatively or positively) NW growth area that can be virtually of any shape due to the programmable ability of FIB technique, the positioning ability of which is more versatile than lithography-based techniques. Interestingly, drastic improvement on vertical-alignment is also achieved for NWs grown on c-plane Al_2O_3 or silicon substrate through our method. We examine the growth kinetics and rate-controlling mechanisms of our approach through a series of control experiments. For practical utility purposes, we observe a variation of photoluminescence properties of our ZnO NWs by simple FIB treatment. As a direct result of substantial enhancement in NWs uniformity (in both diameters and heights), we report enhanced electric current and power generation in our latest version of hybrid ZnO NW generators.[14]

▪ EXPERIMENTAL SECTION

Catalyst Film Preparation: 1.5 nm Au catalyst film was coated on sapphire or silicon substrate using electron-beam evaporation method with a constant deposition rate of 0.01 nm/s. The as-deposited Au film was selectively exposed to Ga^+ ion beam using a Quanta 3D dual beam FIB system (Oregon, USA). The accelerating voltage is 30 KeV. The etching depths were set to 1 nm and the duration time varies from tens of microseconds to several seconds. Patterns with desirable sizes and shapes were preprogrammed during the FIB etching process. For Au-Ga alloy catalyst, 0.5 nm Ga and 1 nm Au film was sequentially evaporated using e-beam evaporation without breaking the vacuum. Pure Au and Ga catalyst films with the same thickness of 1.5 nm were also deposited for comparison purposes.

Nanowire Array Synthesis: ZnO NWs were grown using a double-tube CVTC system equipped with Lindberg blue tube furnace. The diameters of the outer and inner tubes are 2.54 cm and 1.25 cm, respectively, and the lengths are 65 cm and 32.5 cm, respectively. Prior to NW growth, the temperature inside the furnace was carefully calibrated using a K-type thermocouple (TES 1310, Taiwan). An alumina boat (2.8 cm × 0.7 cm × 0.7 cm) containing 782.2 mg ZnO (Alfa Aesar 99.99%) and graphite (200 mesh, Alfa Aesar 99.9%) mixed powders (mass ratio: 1:1) were loaded into the inner tube and

positioned at the center of the outer tube. A-plane or c-plane sapphire substrate coated with catalyst films were directly placed on top of the powders. Ar (99.999+%) was used as the carrier gas at a constant flow rate of 12 sccm. The furnace was heated to the target temperatures (i.e., 880-940 ^{o}C) with a ramping rate of 50 ^{o}C/min., and the holding time is 0.5-5 mins. All NWs were grown in atmospheric environment.

Structural Characterizations: Energy dispersive spectroscopy (EDS) was applied to analyze the compositions of the catalyst film. The ZnO NW morphologies were characterized using a field-emission scanning electron microscope (SEM, FEI, Quanta FEG). The length and diameter were manually measured from a series of SEM images after growth. In the case that the NWs are tapered, the diameter was measured at 2/L position (L is the length of NWs). The crystallographic orientations of as-grown ZnO NWs were characterized using a D8 x-ray diffractometer (XRD) (Brukes). The atomic structures of NWs were examined using a Philips CM 300 transmission electron microscope (TEM) at an accelerating voltage of 300 kV. Room temperature photoluminescence (PL) spectra were collected using a Fluorolog-3 type spectrofluorometer equipped with He-Cd laser.

Fabrication of Nanogenerators: Vertically-aligned ZnO NW arrays catalyzed by Au-Ga film or Au film were chosen to fabricate nanogenerators. For device fabrication, 1% percent Poly (methyl methacrylate) (PMMA) polymer dissolved in toluene was spin-coated to the NW forest. After drying the PMMA film at room temperature, the top surface was oxygen plasma etched in order to expose the NW tips, which was examined by SEM to make sure that NWs protrude from the polymer surface and the exposure length of NWs is nearly the same for each device. To make top electrical contact, 5 nm Ti/200 nm Au film was deposited via e-beam evaporation. Ag paste attached to the ZnO film serves as the bottom electrode.

Nanogenerator Power Conversion: Electrical transport properties of each nanogenerator were examined using Keithley 4200 semiconductor characterization system. For power generation, the

nanogenerator was placed on a Peltier hotplate and heated up from room temperature to 60 ^{o}C. Temperatures were controlled by varying the input voltage of the hotplate. The swelling of PMMA under high temperatures will cause the embedded ZnO NWs to deform and thus piezoelectric voltage (current) signals can be produced. The voltage or current signals were recorded by monitoring electric signals between the top and bottom electrodes while setting the input power as "0".

▪ RESULTS AND DISCUSSION

FIB-patterned uniform NWs. Fig. 1B shows a low magnification scanning electron microscopy (SEM) image of ZnO NW arrays grown on Au-coated (1.5 nm) a-plane Al_2O_3 ($R\bar{3}c$ space group, a=4.758 Å, c=12.991 Å) substrate at 910 ^{o}C for 5 mins., with FIB-treated (30 KeV, 0.19 nA, 1 s) area defined in a circular shape (~50 μm in diameter). The NWs uniformity and quality are better revealed from 45^{o}-tilted and top-view (insets) SEM images taken from the treated, Fig. 1C, and untreated area, Fig. 1D, respectively. Several important features are noteworthy from these images: First, NWs preferentially grow in the FIB exposed area, resulting in substantially taller (~4 μm) NWs than the unexposed area (~0.5 μm). The height of NWs in FIB-treated area is also much more uniform, evident from the more homogeneous top-view contrast of NWs (compare Fig. 1C to Fig. 1D). Second, the diameter-distribution histogram from two areas shown in Fig. 1E illustrate that NWs in FIB-treated area have overall large diameters but an exceedingly narrow size distribution with nearly all NWs in the range of 100-120 nm. In contrast, a wide size distribution is observed in the unirradiated area, with NW diameters ranging from 50-140 nm. The density of NWs in FIB-treated and untreated areas is ~15 /μm^2 and ~17 /μm^2, respectively. Third, the crystal quality in Ga+ implanted region is substantially improved compared to the untreated region, as indicated by the microbeam X-ray diffraction (XRD) pattern (~10 μm diameter beam size) (Fig. 1F) and room temperature photoluminescence (PL) measurements (Fig. 1G). According to Fig. 1F, predominant (0002) diffraction peak is observed in the FIB-treated region, indicative of c-oriented growth and high degree of vertical-alignment. By comparison, the (0002) peak

is weakened and a small ($10\bar{1}1$) diffraction peak is detected in the untreated area under our current growth conditions, suggesting that some NWs grow along other orientations. The photoluminescence spectra in Fig. 1G indicate that the defect-related green emission band centered on ~520 nm is greatly suppressed in FIB-exposed region, suggestive of much higher NWs quality. This observation is in line with some early reports that the higher surface area to volume ratio of smaller diameter NWs (<50 nm) favors a higher level of surface and sub-surface oxygen vacancies.[19] The substantial amount of smaller diameter NWs in the unirradiated area might be the primary reason why the photoluminescence spectrum shows a much stronger green emission peak. These results demonstrate that simple FIB treatment can be applied to tune the optoelectronic properties of ZnO NWs, which could be especially effective if different optical emission is needed with NWs aligned on the same substrate.

At 30 KeV, Ga^+ ions penetrate through the Au layer (1.5 nm thick), and stop primarily in the Al_2O_3 substrate [Supporting Information (SI), Fig. S1].[26] In addition, an appreciable amount of vacancies (~400 per Ga ion) are generated in the target. Implanted Ga is measurable by SEM energy dispersive spectroscopy (EDS) (SI, Fig. S2). We therefore hypothesize that the growth of NWs in FIB-treated area is catalyzed by Au-Ga alloy instead of pure Au, which may have fundamental impacts on the growth kinetics and/or mechanisms of these NWs, as pseudobinary system (Au-Ga)-Zn has completely different eutectic points[27] than those of binary Au-Zn. In addition, surface atomic steps or defects generated by Ga^+ sputtering may influence the growth rate as surface steps or kinks enhance nucleation probability of deposited materials.[28] Our control experiments at the low temperature (880 ^oC) indicate that denser nucleation sites were formed in the FIB-treated region (SI, Fig. S3), suggesting easy nucleation processes. When the FIB etching time was prolonged (30 KeV, 0.3 nA, 2 s), however, NWs could become tilted from the substrate. Further FIB etching (30 KeV, 0.3 nA, 8 s) completely removes Au film, and ZnO NWs are no longer able to grow (SI, Fig. S4). These informative experiments underscore the dual importance of both Au and Ga implantation on the observed growth behavior. Due to the programmable ability of FIB technique, a wide range of sophisticated growth patterns can be readily

created; two examples are illustrated in SI, Figs. S5-S6. We thus believe that our approach could be useful for optoelectronic applications, which is likely more suitable for single devices (instead of large scale fabrication – an area that traditional lithography patterning prevails).

Vertical-alignment on nonepitaxial substrates. The vertical-alignment growth is of fundamental importance to device utilities, including optoelectronics, nanogenerators, sensors, and field-emitters. [29] Traditionally, two major approaches have been applied to achieve high-quality vertical growth of ZnO NWs; i.e., heteroepitaxial growth on epitaxial single-crystalline substrates such as GaN or a-plane Al_2O_3,[14, 16, 19, 30] and homoepitaxial growth by using textured ZnO seeding layers.[8] The former is relatively expensive and involves isolating substrates; the later follows a nontrivial two-step process that sometimes has residual contamination issues. Other vertical alignment strategies have also been reported; but they were often hit-and-miss.[22, 31] Interestingly, we observe that vertical-alignment growth was achieved in the FIB-treated c-plane Al_2O_3 substrate (a nonepitaxial substrate for ZnO),[30] as illustrated in Fig. 2A, where random-alignment is seen in regions outside the FIB-treated circle. This interesting result suggests that vertical alignment may be achievable on nonepitaxial substrates via Au-Ga alloy catalyst. The SEM images shown in Figs. 2B and 2C support this hypothesis, which indicate that near-perfect vertical-alignment is obtained when using 1 nm Au/0.5 nm Ga catalyst on c-plane Al_2O_3 substrate (Fig. 2B), whereas random alignment is seen for 1.5 nm pure Au catalyst (Fig. 2C). In addition, the Au-Ga catalyzed sample shows a much narrower length (~1.2-1.8 μm) distribution compared with that of Au-catalyzed sample (~1.2-4.3 μm), with the average diameter of Au-Ga sample slightly larger. XRD patterns in Fig. 2D confirm the preferential c-oriented growth of Au-Ga catalyzed sample, in contrast to relatively misoriented growth nature of Au sample. Moreover, such vertical-alignment is achieved in the entire temperature range we have investigated (i.e., 880-920 ^{o}C). The transmission electron microscopy (TEM) examinations of ZnO NWs grown from Au-Ga catalyst, shown in Figs. 2E-G, indicate that the growth front of many NWs is in semi-round shape without any catalyst. High-resolution TEMs from the tip (Fig. 2F) and edge (Fig. 2G) of a NW show atomically

smooth surface without clear evidence of defects, consistent with the high-quality nature of NWs. These intriguing experimental results strongly suggest that the growth mechanisms of ZnO NWs may be fundamentally different when catalyzed by Au-Ga alloys compared to the commonly studied Au catalyst.

To understand the origin of vertical-alignment, we examine the incubation (i.e., nucleation) period of ZnO on c-plane Al_2O_3 substrate by using Au-Ga and Au films at two temperatures (880 ^oC and 900 ^oC), respectively. The growth time is fixed at 30 s for all the cases. The comparison results are displayed in SI, Fig. S7. The film breakup and formation of isolated ZnO textured seeds are observed for Au-Ga catalyst, SI, Figs. S7A-B. This is not surprising, considering the low eutectic point of Au-Ga alloy (at 339 ^oC), suggesting that the film has become liquid phase before the Zn vapor is transported to the surface. In contrast, the Au film remains nearly intact during the initial growth; i.e., Zn vapor seems directly absorbed by solid Au film, SI, Fig. S7C. The further growth may proceed with the formation of ZnO seeds, and the majority of NWs grow 51.8^o-oriented off the c-plane sapphire substrate following the $[0001]_{ZnO}||[10\bar{1}4]_{sapphire}$ and $[10\bar{1}0]_{ZnO}||[1\bar{2}10]$ epitaxy,[30] SI, Fig. S7D. XRD patterns (SI, Fig. S7E) further indicate that the ZnO seeds from Au-Ga catalyst have a preferred {0002} orientation that may be the primary reason why vertical-alignment growth was obtained for Au-Ga catalyzed samples.

Growth mechanisms and kinetics. Although the growth of ZnO NWs has been broadly investigated,[3, 5, 7, 8, 12, 21-24, 30, 32-43] the understanding of *alloy catalysts* on the growth behavior is surprisingly rare and seldom studied. *To our knowledge, there are no previous studies on Au-Ga catalyst for ZnO NWs growth;* but such studies could be very beneficial due to less contamination nature of alloys compared to pure noble metals. In addition, the fundamental growth kinetics and mechanisms of ZnO NWs can be quite complex. To comprehend the enhancement in NWs quality, uniformity, vertical-alignment, and elucidate the rate-controlling factors in NW growth, we carried out a series of comparison experiments at different temperatures (880-940 ^oC) by using pure Au (~1.5 nm) and Au-Ga (~1 nm Au and ~0.5 nm Ga) thin films as catalysts, respectively. As shown in Figs. 3A-H, it is plain that

ZnO NWs have higher quality at all growth temperatures when using Au-Ga catalyst (compared to Au), and that NWs can grow at a lower temperature (~880 ^{o}C) for Au-Ga catalyst, Fig. 3A, consistent with the very low eutectic points of Au-Ga-Zn ternary system. Note that the CVTC process relies on a reduction of ZnO powder and the evaporation of Zn which limits the lowest temperature we could investigate. Our thermogravimetric analysis (TGA) suggests that Zn and C have a reaction temperature of ~880 ^{o}C at a heating rate of ~ 20 ^{o}C/min., SI, Fig. S8. Interestingly, we observe an inverse temperature-dependent diameter trend for both catalysts; i.e., the average diameter of NWs first increases with the growth temperature, reaches a maximum value (900 ^{o}C for Au, and 920 ^{o}C for Au-Ga, see Figs. 4E, F), and tails off as the temperature further rises. These results imply that there exists an optimal temperature for NWs to grow under the current thermal reduction process, and that the NW diameters may not be completely defined by the initial catalyst sizes, suggesting the perversely complex nature of NWs growth.[44]

The growth kinetics or the rate-controlling steps of NW growth for two catalysts can be better revealed through the length (L) vs. diameter (*d*) statistic trends displayed in Figs. 4A-D. For the convenience of comparison, the growth time for all samples is set to 1 min. Here the growth rate (V=dL/dt) is simply calculated via L divided by total growth time (i.e., include incubation time of NWs). For the CVTC synthesis of ZnO NWs, several key rate-limiting steps could contribute to the NW growth (assuming VSS or VLS processes): (1) the Zn vapor transportation to the surface; (2) the incorporation of Zn vapor into the catalyst via vapor-solid or vapor-liquid interface;[45] (3) diffusion of source materials in the solid or liquid phase; and (4) nucleation of source materials from solid/solid or liquid/solid or liquid/solid/vapor interfaces. Note that step (4) may also involve the oxidation of Zn. Steps (2) and (4) typically lead to a positive slope in L vs. *d* plot due to the classical Gibbs-Thomson effect or nucleation controlled growth mechanisms, whereas steps (1) and (3) render a negative slope (i.e., growth rate decreases with diameter). In Figs. 4A-D, we note that the slope of L-*d* for Au catalyst

remains positive and increases with growth temperatures, Fig. 4E, suggesting that the growth via Au catalyst is kinetics controlled. The growth rate of NWs can be expressed as Arrhenius-type equation

$$V = K_0 e^{-E_a/kT}, \qquad (1)$$

where K_0 is the pre-factor, E_a activation energy, *K* Boltzmann constant, and T the temperature. A linear-least-square fit of the growth rates at different temperatures shown in SI, Fig. S9A yields an E_a of 3.22 eV for the Au catalyst. Note that this value is obtained by including the incubation time of NWs, which is surprisingly higher than the activation energy of various processes seen in ZnO materials, Table 1.[46-52] The wide spread of the activation energy data in the literature indicates the complexity of growth kinetics and testify that a united picture on fundamental growth process of ZnO NWs has not reached yet. In fact, our E_a is close to the ZnO bulk diffusion activation energy (~3.16 eV),[46] which may suggest that the initial growth (i.e., the first 1 min.) of ZnO NWs is primarily related to the vapor-solid (VS) nucleation process instead of the commonly believed VLS process.[19] This may also be attributed to the fact that all the growth temperatures studied here are below the melting temperature of Au, and that the incubation time for low temperature is relatively long. For example, we observed a 30 s incubation time for the 880 ^{o}C case. By taking into account the incubation time at different temperatures, which are 30 s, 20 s, 15 s, and 10 s for 880 ^{o}C, 900 ^{o}C, 920 ^{o}C, 940 ^{o}C, respectively, we obtain an activation energy of 2.20 eV for the growth with Au catalyst – a value that is in line with those reported in the literature for similar CVTC processes.[53] Due to the relatively large scattering of the L-*d* data and the facts that mixed growth mechanisms are often seen in Au catalyzed ZnO NW growth,[36] we refrain from further discussions of the underlying physical mechanisms.

On the other hand, as illustrated in Fig. 4F, the growth rate of NWs catalyzed with Au-Ga increases first and then drops after 920 ^{o}C. This suggests that the growth behavior may not be controlled by kinetics at the highest temperature. By using the first three temperatures, we estimated an E_a of 2.82 eV (SI, Fig. S9B), which is lower than that for the case of growth on Au catalyst. This agrees with the easier growth nature of NWs with the Au-Ga catalyst. Interestingly, we further note that the slope of L-*d*

for Au-Ga catalyst shifts from positive to negative as the temperature arises. A negative slope at 940 ^{o}C for Au-Ga catalyst is a hallmark of source- or diffusion-limited growth process [i.e., (1) or (3) step above].[54] This slope transition may allow us to locate a temperature region where the growth rate of NWs can be independent of diameter (i.e., zero slope) – a vital route to narrow the NW height distributions.[54] For Au-Ga catalyst, this temperature is likely between 920-940 ^{o}C (see Fig. 4C and 4D). Due to the exceptionally narrow distribution of ZnO NWs grown from FIB-treated Au catalyst (see Fig. 1E), the growth rate of this sample at 910 ^{o}C is essentially diameter-independent. The slightly lower temperature seen in FIB sample compared to that expected from Au-Ga catalyst is not surprising, as catalyst composition discrepancy exists between these two samples.

Experimentally, we also observe a layer of porous ZnO film underneath NWs for Au-Ga catalyst at higher temperatures (SI, Fig. S10), which appears to suggest the Stranski-Krastanov growth mode.[31] The high sticking coefficient of liquid phase may allow for the formation of a textured ZnO wetting layer prior to NW growth – a mechanism that was proposed in the literature.[8, 19] Our controlled experiments have indeed revealed a thin layer of ZnO seeding layer at 940 ^{o}C (SI, Fig. S11), after which NWs were seen to grow. At the growth temperatures below 920 ^{o}C, however, we only observed isolated ZnO seeds (see SI, Fig. S7A). This leads us to speculate that the growth at lower temperatures may follow the Volmer-Weber mechanism,[55] and that the seeding film is not prerequisite to vertical-alignment. Interestingly, Au-Ga catalyst was not found on the tips of ZnO NWs at all growth temperatures, indicating that the growth of NWs may proceed through a self-catalyzed process.[22] The role of Au-Ga catalyst seems to act as source to adsorb Zn vapor and the nucleation of ZnO seeds. Two additional observations further support this hypothesis: (1) an inverse tapering behavior is observed at 940 ^{o}C for Au-Ga catalyst; i.e., the bottom half of NWs is thinner than the top half (inset of Fig. 3H). This is not consistent with conventional VLS processes as a normal tapering behavior is expected for such a process; (2) the growth rate at 940 ^{o}C is slower than those at lower temperatures, plus a negative

L-*d* slope. This is a strong indication that surface-diffusion along the NW sidewalls controls the NW growth at this temperature.

Questions remain on why the ZnO seeds have preferred texture (see SI, Fig. S7E).[56] Some calculations suggest that the {0001} surface energy of ZnO depends upon the crystal thickness so that a thin slab (i.e., ZnO nuclei) could adopt the {0001} orientation,[57] which maintains its crystallographic orientation during further growth as {0001} is the highest-energy but fast grown surface.[30] In our case, however, we suspect that the high affinity of Ga to oxygen may play a role in the ZnO seed formation and promote the c-axis texturing. We argue that the interfacial energy between the substrate and the seeding layer could influence the texture orientation of ZnO, provided that the textured seeds are formed on the substrate – catalyst interfaces. To test this hypothesis, we replace c-plane Al_2O_3 with a (100) silicon substrate (with 250 nm native oxide layer) and grow NWs with the same composition Au-Ga catalyst. We find that the vertical alignment of ZnO NWs is achieved (SI, Fig. S12); but is clearly worse than in the case of the c-plane Al_2O_3 substrate. Note and it has been suggested in the literature[58] that the achievement of vertical alignment can be helped by the formation of Al_2ZnO_4 nanostructures, which requires the diffusion of Zn and O into Al_2O_3 that takes time and also strongly depends upon the growth temperature. This is an unlikely scenario in our cases due to the very short growth time used in our experiments.

Nanogenerators with enhanced power output. The facile synthesis of vertically-aligned ZnO NWs with much better controlled length and diameter uniformity is expected to be beneficial for optoelectronic applications, including solar cells.[2, 15] In addition, ZnO NWs are important building blocks for piezoelectric nanogenerators.[29, 37] Although continuously increased conversion efficiency and power output have been reported for ZnO NW based nanogenerators, most piezoelectric nanogenerators focus on the mechanical energy conversions. The platforms that are able to harvest non-mechanical energy sources are desirable in order to broaden the applications of nanogenerators and convert multiple environmental energies; but have been progressing slowly. We have recently developed the first

generation piezoelectric/polymer hybrid nanogenerators,[14] where vertically aligned ZnO NWs are embedded inside polymer matrix (SI, Fig. S13). In principle, such devices can harvest multiple energies (light, pressure, chemical energy) through stimulus mechanisms on polymers. As a proof-of-concept, we demonstrate that our protocol platforms can convert thermal energy into electricity by taking advantage of the shape change of thermoplastic polymers and the axial deformation of NWs (in contrast to the bending motion of NWs in most nanogenerators). Despite the advantages of converting non-mechanical energies using piezoelectric transducers, it has been difficult and challenging to enhance the power output of these nanogenerators. Quantitatively and for the first-order approximation, the piezoelectric potential of such a device can be given by[14]

$$U=\frac{A_p E_p}{A_p E_p + A_n E_n}(\alpha_p - \alpha_n)\Delta T \frac{1}{d_{33}}, \qquad (2)$$

where A, E, α refer to areal fraction, Young's modulus, thermal expansion coefficient, respectively. The subscript ′p′ and ′n′ represent polymer and NWs, respectively. ΔT is the temperature change, and d_{33} is the piezoelectric constant of ZnO along the Z-axis. The equation adequately predicts the voltage output trend and its correlations with the mechanical and physical properties of polymers (e.g., stiffness and thermal expansion coefficient). However, it does not take into account of many other important variables such as the electrical properties and geometric factors of NWs, interfacial coupling strength between NWs and polymer,[59] and the alignment of transducers. If these factors can be fully understood, a substantial enhancement of power generation is possible. Intuitively, more uniform NWs could not only facilitate device fabrication, but also help enhanced power generation (to be discussed in the next paragraph). But such approach is challenging due to the difficulty of controlling NW size distributions.

Here we report drastic increase in power generation by tuning the NW diameter distributions, using the new catalyst we have developed. Two nanogenerators, with ZnO NWs grown via Au-Ga and Au catalysts, respectively, were fabricated according to the procedures described in Ref. [14].[14] The power generation ability of the devices was tested using a thermal stimulator (i.e., a Peltier heater), and is compared in Fig. 5. In the same device area (~1 mm^2), the peak electric current output of Device A

fabricated from Au-Ga catalyzed NWs is about twice of that from Device B (which used Au-catalyzed NWs), suggesting the higher power generation ability of Device A (which used Au-Ga catalyzed NWs). Based on the open circuit voltage and the electric current, we calculate a peak power generation of 1.64 nW and 0.64 nW for Devices A and B, respectively; i.e., a 2.5-fold increase in power generation. This is quite significant, considering that about 55% of heat on the earth is wasted. we believe such power enhancement could be benefit from several important factors: (1) more uniform NW geometries and densities in A (see Fig. 5A vis-à-vis Fig. 5B), which make the fabrication of electrode contacts much easier; (2) nearly all ZnO NWs in Device A are aligned along the {0002} direction, which is the orientation with the highest piezoelectric constant, whereas some NWs are grown along other orientations in Device B; (3) the ZnO NWs from Au-Ga catalyst have fewer defects. Perhaps even more importantly, the vertical-alignment of ZnO NWs achieved via the alloy catalyst allows us to fabricate nanogenerators on a variety of flexible substrates, which is otherwise not possible via conventional Au-catalyst approach. Patterning or even 3-D printing of nanogenerators could become possible due to the versatility and programming ability of the FIB technique.

▪ CONCLUSIONS

We have demonstrated a FIB-assisted control growth of ZnO NWs with very narrower diameter distributions, height uniformity, and better crystalline quality. Vertical-alignment is achieved with this technique, together with programmable patterning capability. Comparison studies of ZnO NWs growth in the temperature range of 880-920 ^{o}C with Au and Au-Ga catalysts reveal different growth kinetics and mechanisms. It was found that the growth of NWs on Au film is kinetics controlled with an activation energy of 2.20-3.22 eV. In contrast, the growth controlling mechanisms for the Au-Ga catalyst depends on the temperature. The lack of catalyst on NWs tips and a negative L-*d* slope suggest that the growth of these NWs at higher temperatures is self-catalyzed with the growth behavior controlled by self-diffusion processes. A narrow NW size distribution is achievable for Au-Ga alloy catalyst. Nanogenerators have been fabricated based on the knowledge learned from our growth studies.

High quality and high uniform NW platform generates a current output that is approximately doubled compared to that achieved in our previous approach. Other applications of FIB-assisted or Au-Ga catalyzed growth could include sensors, field emitters, optoelectronics, and light-emitting diodes that rely heavily on NW dimensional control and vertical-alignment.

Supporting Information Available: Supporting Figures S1-S13. This material is available free of charge via the Internet at http://pubs.acs.org.

AUTHOR INFORMATION

X.Y.W., S.F.X., J.L. and Y.M.W. carried out experiments. S.O.K. contributed to the calculation of Ga+ ion implantation depth profile. Y.M.W. wrote the manuscript with valuable inputs from X.Y.W. and S.O.K.

ACKNOWLEDGEMENT

The authors would like to thank helpful discussions of Drs. Deng Pan (USST), Alex Chernov (LLNL), and Luis Zepeda-Ruiz (LLNL). The work at USST is supported by NSFC (51072119), Shanghai Project no. 10540500900, and Innovation Program of Shanghai Municipal Education Commission (12ZZ139). The work at LLNL was performed under the auspices of the U.S. Department of Energy by Lawrence Livermore National Laboratory under Contract No. DE-AC52-07NA27344. Y.M.W is partially supported by the LDRD Programs (12-ERD-053 and 12-FS-011) at LLNL.

FIGURE CAPTIONS

Figure 1. (**A**) The schematic of our approach by using FIB exposure of Au catalyst. (**B**) Preferential growth of ZnO NWs in FIB-treated area (the central circle). (**C**) and (**D**), plan-view SEM images of the NWs from the region exposed to FIB, and unexposed, respectively. The insets are 45°-tilted view images for (C) and (D), respectively. (**E**) Diameter distributions from FIB-treated and untreated regions, showing vast difference in terms of diameter uniformity. (**F**) and (**G**), XRD and room-temperature photoluminescence spectra of NWs from FIB-treated and untreated areas, respectively.

Figure 2. ZnO NWs and their microstructure grown on c-plane Al_2O_3 substrate. (**A**) The vertical-alignment of ZnO NWs observed in FIB-treated area (middle circle). The FIB condition was 30 KeV, 0.3 nA, 0.7 s. The NWs were grown at 910 °C for 1 min. (**B**) and (**C**), SEM images of vertically- and randomly-aligned ZnO NWs grown (910 °C, 2 mins.) with Au-Ga and Au catalysts, respectively. (**D**) XRD patterns of ZnO NWs from (B) and (C), respectively. (**E**) A TEM image of ZnO NWs grown with Au-Ga catalyst. The square area highlights the semi-round shape of a NW. (**F**) and (**G**), zoomed-in high-resolution TEM images from the tip (F) and edge (G) of the ZnO NW shown in (E).

Figure 3. A comparison of ZnO NW morphologies grown with Au and Au-Ga catalysts. All the images have the same scale bar except for the inset. (**A**)-(**D**), SEM images of ZnO NWs grown with Au catalyst, at 880, 900, 920, 940 °C, respectively. (**E**)-(**H**), morphologies of ZnO NWs grown with Au-Ga catalyst, following the same temperature order as Au. The growth time for all images is 1 min. The inset in (H) is a zoomed-in SEM image of a NW with 200 nm scale bar.

Figure 4. Length (L) vs. diameter (*d*) plots of ZnO NWs grown with Au and Au-Ga catalysts at the temperature of (**A**) 880 °C, (**B**) 900 °C, (**C**) 920 °C, and (**D**) 940 °C, respectively. The straight line in each figure is the least-square fit line for the set of L-*d* data (>100 counts) at that temperature. (**E**) and (**F**), the average growth rate (V) and the average diameter at different growth temperatures for Au and Au-Ga catalysts, respectively.

Figure 5. (**A**) and (**B**), SEM images of the top surfaces of nanogenerators after oxygen plasma etching before the electrode contacts were made, for Au and Au-Ga grown ZnO NWs, respectively. The NW density is estimated to be ~15 /μm^2 and ~17 /μm^2 for (A) and (B), respectively. (**C**) and (**D**), electric currents generated from the devices in (A) and (B), respectively. A Peltier heater (defined as the heating voltage in the figures) was used to thermally stimulate the nanogenerators in order to simulate the power generation capability.

TABLE 1 A partial list of activation energies reported in the literature on ZnO NW growth (CVTC: chemical vapor transport and condensation; PVD: physical vapor deposition)

Synthesis Conditions	Activation Energy (E_a, eV)	Proposed Mechanisms	References	Note
CVTC with ZnO+C as precursors, Au particles as catalyst, 900 ^oC	1.73-2.62	Surface diffusion controlled	[53]	E_a is diameter dependent
CVTC with ZnO+C as precursors, Au as catalyst, 880-940 ^oC	3.22	--	Our work	Including incubation time
	2.20	--		Growth only
CVTC with ZnO+C as precursors, Au-Ga as catalyst, 880-920 ^oC	2.82	--	Our work	
Heating Zn in air, no catalyst, 400-530 ^oC	0.87	Migration of Zn interstitials	[46]	
PVD with ZnO powder, no catalyst, 1000-1400 ^oC	1.33	Oxidation of Zn	[12, 47]	
--	3.16	ZnO lattice diffusion	[48]	Not related to NW growth
--	2.46	The activation energy for the formation ZnO	[52]	Not related to NW growth
Hydrothermal, 60-140 ^oC, on GaN substrate	0.77-2.11	--	[51]	Model prediction (E_a is length and density dependent)
CVTC with ZnO+C as precursors, on amorphous carbon, no catalyst, 785-860 ^oC	2.43	Formation of ZnO	[50]	E_a is diameter dependent

Figure 1

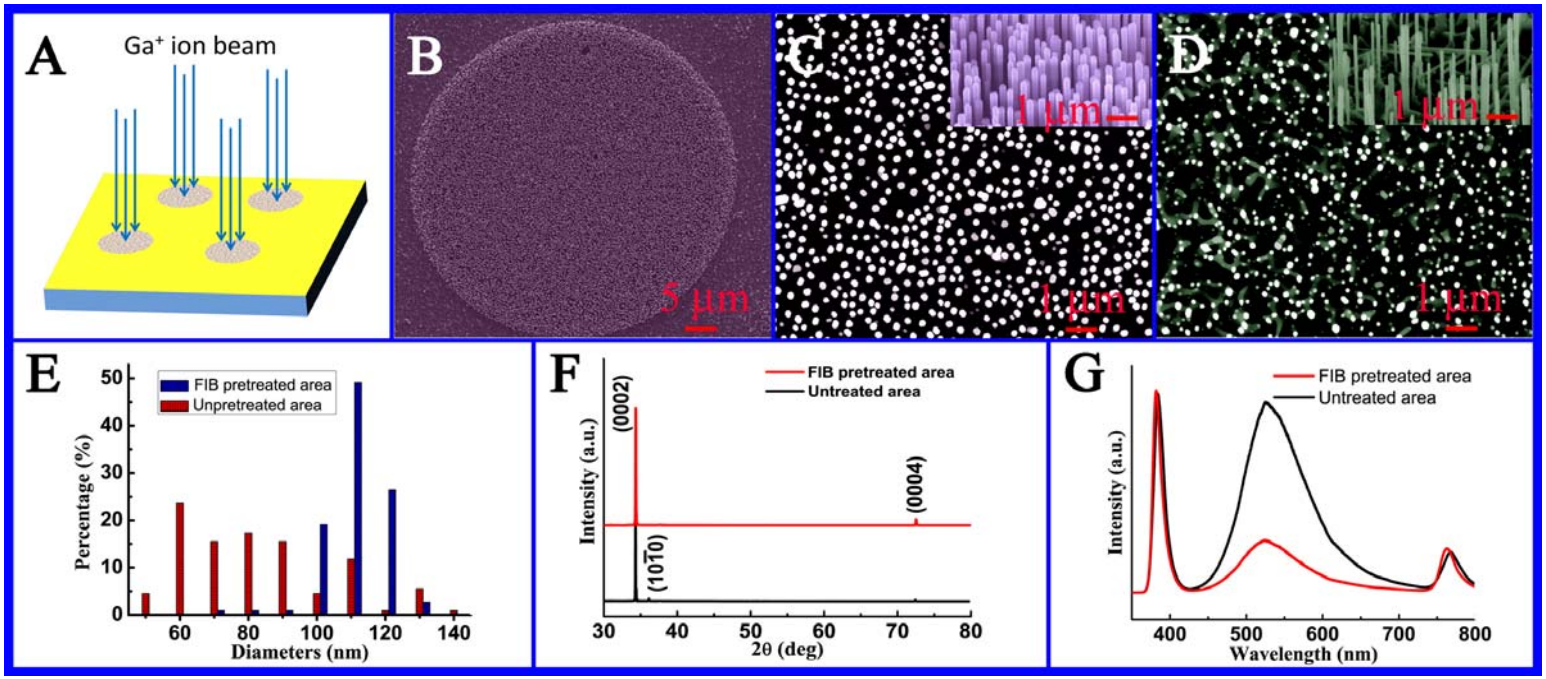
A
Ga+ ion beam
B
5 μm
C
1 μm
1 μm
D
1 μm
1 μm
E
FIB pretreated area
Unpretreated area
Percentage (%)
Diameters (nm)
F
FIB pretreated area
Untreated area
(0002)
(0004)
(10$\bar{1}$0)
Intensity (a.u.)
2θ (deg)
G
FIB pretreated area
Untreated area
Intensity (a.u.)
Wavelength (nm)

Figure 2

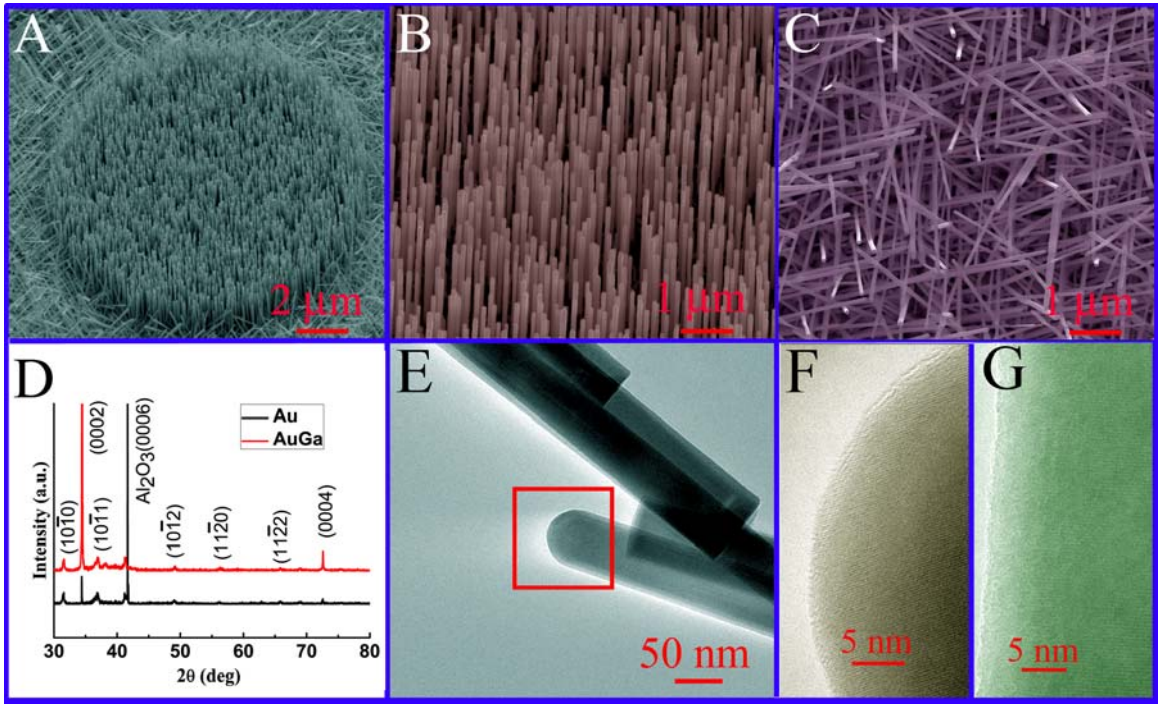
A
2 μm
B
1 μm
C
1 μm
D
Au
AuGa
Intensity (a.u.)
(10$\bar{1}$0)
(0002)
(10$\bar{1}$1)
Al2O3(0006)
(10$\bar{1}$2)
(11$\bar{2}$0)
(11$\bar{2}$2)
(0004)
30
40
50
60
70
80
2θ (deg)
E
50 nm
F
5 nm
G
5 nm

Figure 3

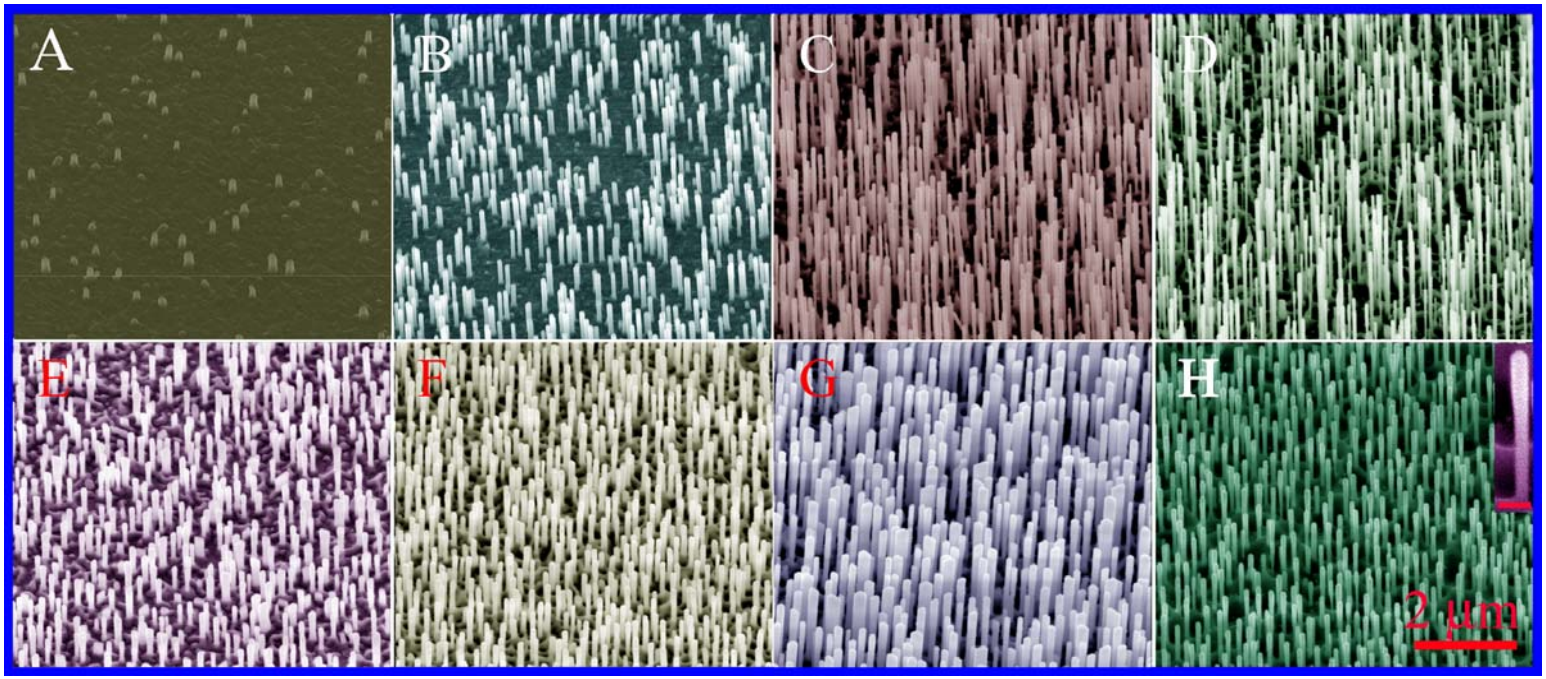

Figure 4

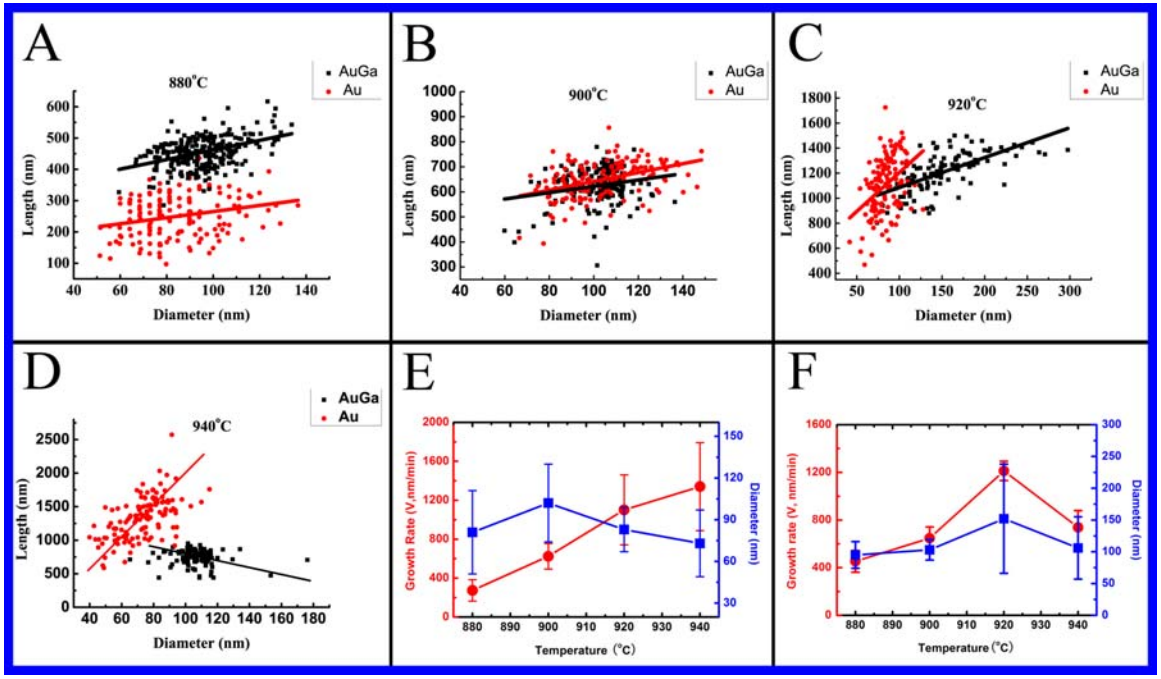
A
880°C
AuGa
Au
Length (nm)
Diameter (nm)
B
900°C
AuGa
Au
Length (nm)
Diameter (nm)
C
920°C
AuGa
Au
Length (nm)
Diameter (nm)
D
940°C
AuGa
Au
Length (nm)
Diameter (nm)
E
Growth Rate (V,nm/min)
Diameter (nm)
Temperature (°C)
F
Growth rate (V, nm/min)
Diameter (nm)
Temperature (°C)

Figure 5

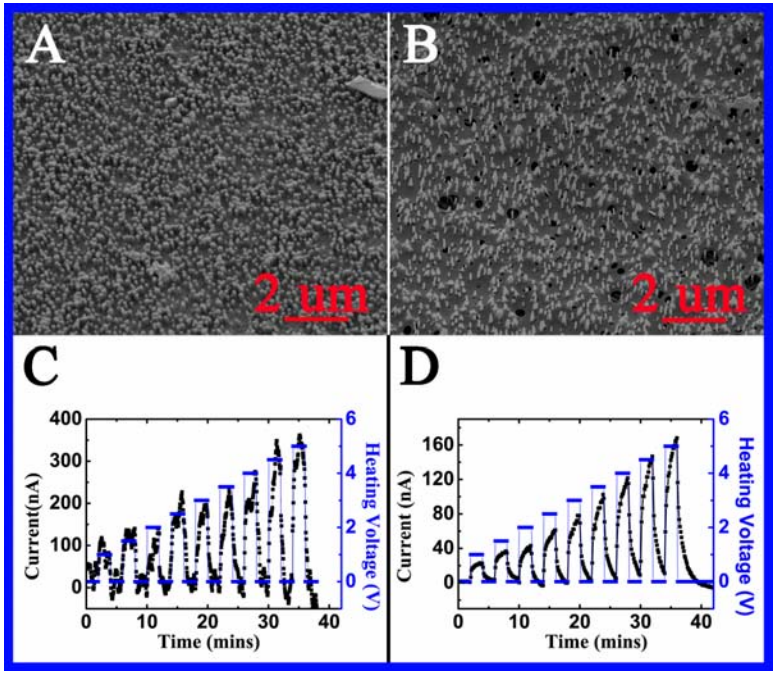
A
2 um
B
2 um
C
Current(nA)
Heating Voltage (V)
Time (mins)
D
Current (nA)
Heating Voltage (V)
Time (mins)

REFERENCES

1. Xu, S.; Wang, Z. L., One-dimensional ZnO nanostructures: Solution growth and functional properties. *Nano Res.* **2011,** 4 (11), 1013-1098.

2. Law, M.; Greene, L. E.; Johnson, J. C.; Saykally, R.; Yang, P. D., Nanowire dye-sensitized solar cells. *Nature Mater.* **2005,** 4 (6), 455-459.

3. Yuan, G. D.; Zhang, W. J.; Jie, J. S.; Fan, X.; Zapien, J. A.; Leung, Y. H.; Luo, L. B.; Wang, P. F.; Lee, C. S.; Lee, S. T., p-type ZnO nanowire arrays. *Nano Lett.* **2008,** 8 (8), 2591-2597.

4. Xiang, B.; Wang, P.; Zhang, X.; Dayeh, S. A.; Aplin, D. P. R.; Soci, C.; Yu, D.; Wang, D., Rational synthesis of p-type zinc oxide nanowire arrays using simple chemical vapor deposition. *Nano Lett.* **2007,** 7 (2), 323-328.

5. Tian, Z. R. R.; Voigt, J. A.; Liu, J.; McKenzie, B.; McDermott, M. J.; Rodriguez, M. A.; Konishi, H.; Xu, H. F., Complex and oriented ZnO nanostructures. *Nature Mater.* **2003,** 2 (12), 821-826.

6. Joo, J.; Chow, B. Y.; Prakash, M.; Boyden, E. S.; Jacobson, J. M., Face-selective electrostatic control of hydrothermal zinc oxide nanowire synthesis. *Nature Mater.* **2011,** 10 (8), 596-601.

7. Wei, Y.; Wu, W.; Guo, R.; Yuan, D.; Das, S.; Wang, Z. L., Wafer-Scale High-Throughput Ordered Growth of Vertically Aligned ZnO Nanowire Arrays. *Nano Lett.* **2010,** 10 (9), 3414-3419.

8. Greene, L. E.; Law, M.; Tan, D. H.; Montano, M.; Goldberger, J.; Somorjai, G.; Yang, P. D., General route to vertical ZnO nanowire arrays using textured ZnO seeds. *Nano Lett.* **2005,** 5 (7), 1231-1236.

9. Kong, X. Y.; Ding, Y.; Yang, R.; Wang, Z. L., Single-crystal nanorings formed by epitaxial self-coiling of polar nanobelts. *Science* **2004,** 303 (5662), 1348-1351.

10. Lao, J. Y.; Huang, J. Y.; Wang, D. Z.; Ren, Z. F., ZnO nanobridges and nanonails. *Nano Lett.* **2003,** 3 (2), 235-238.

11. Vayssieres, L.; Keis, K.; Hagfeldt, A.; Lindquist, S. E., Three-dimensional array of highly oriented crystalline ZnO microtubes. *Chem. Mater.* **2001,** 13 (12), 4395-4398.

12. Shi, J.; Hong, H.; Ding, Y.; Yang, Y. A.; Wang, F.; Cai, W. B.; Wang, X. D., Evolution of zinc oxide nanostructures through kinetics control. *J. Mater. Chem.* **2011,** 21 (25), 9000-9008.

13. Huang, M. H.; Mao, S.; Feick, H.; Yan, H. Q.; Wu, Y. Y.; Kind, H.; Weber, E.; Russo, R.; Yang, P. D., Room-temperature ultraviolet nanowire nanolasers. *Science* **2001,** 292 (5523), 1897-1899.

14. Wang, X.; Kim, K.; Wang, Y.; Stadermann, M.; Noy, A.; Hamza, A. V.; Yang, J.; Sirbuly, D. J., Matrix-Assisted Energy Conversion in Nanostructured Piezoelectric Arrays. *Nano Lett.* **2010,** 10 (12), 4901-4907.

15. Baxter, J. B.; Aydil, E. S., Nanowire-based dye-sensitized solar cells. *Appl. Phys. Lett.* **2005,** 86 (5), 053114.

16. Wang, X.; Wang, Y.; Aberg, D.; Erhart, P.; Misra, N.; Noy, A.; Hamza, A. V.; Yang, J., Batteryless Chemical Detection with Semiconductor Nanowires. *Adv. Mater.* **2011,** 23 (1), 117-121.

17. Goldberger, J.; He, R. R.; Zhang, Y. F.; Lee, S. W.; Yan, H. Q.; Choi, H. J.; Yang, P. D., Single-crystal gallium nitride nanotubes. *Nature* **2003,** 422 (6932), 599-602.

18. Song, T.; Xia, J.; Lee, J.-H.; Lee, D. H.; Kwon, M.-S.; Choi, J.-M.; Wu, J.; Doo, S. K.; Chang, H.; Il Park, W.; Zang, D. S.; Kim, H.; Huang, Y.; Hwang, K.-C.; Rogers, J. A.; Paik, U., Arrays of Sealed Silicon Nanotubes As Anodes for Lithium Ion Batteries. *Nano Lett.* **2010,** 10 (5), 1710-1716.

19. Yang, P. D.; Yan, H. Q.; Mao, S.; Russo, R.; Johnson, J.; Saykally, R.; Morris, N.; Pham, J.; He, R. R.; Choi, H. J., Controlled growth of ZnO nanowires and their optical properties. *Adv. Funct. Mater.* **2002,** 12 (5), 323-331.

20. Kodambaka, S.; Tersoff, J.; Reuter, M. C.; Ross, F. M., Diameter-independent kinetics in the vapor-liquid-solid growth of Si nanowires. *Phys. Rev. Lett.* **2006,** 96 (9), 096105.

21. Tsivion, D.; Schvartzman, M.; Popovitz-Biro, R.; Joselevich, E., Guided Growth of Horizontal ZnO Nanowires with Controlled Orientations on Flat and Faceted Sapphire Surfaces. *ACS Nano* **2012,** 6 (7), 6433-6445.

22. Geng, C. Y.; Jiang, Y.; Yao, Y.; Meng, X. M.; Zapien, J. A.; Lee, C. S.; Lifshitz, Y.; Lee, S. T., Well-aligned ZnO nanowire arrays fabricated on silicon substrates. *Adv. Funct. Mater.* **2004,** 14 (6), 589-594.

23. Greyson, E. C.; Babayan, Y.; Odom, T. W., Directed growth of ordered arrays of small-diameter ZnO nanowires. *Adv. Mater.* **2004,** 16 (15), 1348-1352.

24. Ito, D.; Jespersen, M. L.; Hutchison, J. E., Selective Growth of Vertical ZnO Nanowire Arrays Using Chemically Anchored Gold Nanoparticles. *ACS Nano* **2008,** 2 (10), 2001-2006.

25. Jun, K.; Jacobson, J. M., Programmable Growth of Branched Silicon Nanowires Using a Focused Ion Beam. *Nano Lett.* **2010,** 10 (8), 2777-2782.

26. The calculation software is available online at http://www.srim.org/.

27. The phase diagram of Au-Ga (1990 Massalski T.B.) is free online available at http://www1.asminternational.org/asmenterprise/apd/.

28. Kim, S. W.; Kotani, T.; Ueda, M.; Fujita, S.; Fujita, S., Selective formation of ZnO nanodots on nanopatterned substrates by metalorganic chemical vapor deposition. *Appl. Phys. Lett.* **2003,** 83 (17), 3593-3595.

29. Brewer, J. R.; Deo, N.; Wang, Y. M.; Cheung, C. L., Lanthanum hexaboride nanoobelisks. *Chem. Mater.* **2007,** 19 (26), 6379-6381.

30. Baxter, J. B.; Aydil, E. S., Epitaxial growth of ZnO nanowires on a- and c-plane sapphire. *J. Cryst. Growth* **2005,** 274 (3-4), 407-411.

31. Zhang, H. Z.; Sun, X. C.; Wang, R. M.; Yu, D. P., Growth and formation mechanism of c-oriented ZnO nanorod arrays deposited on glass. *J. Cryst. Growth* **2004,** 269 (2-4), 464-471.

32. Zhu, Z. M.; Chen, T. L.; Gu, Y.; Warren, J.; Osgood, R. M., Zinc oxide nanowires grown by vapor-phase transport using selected metal catalysts: A comparative study. *Chem. Mater.* **2005,** 17 (16), 4227-4234.

33. Ko, S. H.; Lee, D.; Kang, H. W.; Nam, K. H.; Yeo, J. Y.; Hong, S. J.; Grigoropoulos, C. P.; Sung, H. J., Nanoforest of Hydrothermally Grown Hierarchical ZnO Nanowires for a High Efficiency Dye-Sensitized Solar Cell. *Nano Lett.* **2011,** 11 (2), 666-671.

34. Yang, X.; Wolcott, A.; Wang, G.; Sobo, A.; Fitzmorris, R. C.; Qian, F.; Zhang, J. Z.; Li, Y., Nitrogen-Doped ZnO Nanowire Arrays for Photoelectrochemical Water Splitting. *Nano Lett.* **2009,** 9 (6), 2331-2336.

35. Liu, J.; Xie, S. F.; Cao, Y.; Chen, Y. L.; Zeng, H. D.; Yang, J. H.; Liu, F.; Wang, X. Y., Microstructure evolution and enhanced green luminescence in P-doped ZnO nanowires. *Mater. Lett.* **2012,** 70, 80-82.

36. Brewster, M. M.; Zhou, X. A.; Lim, S. K.; Gradecak, S., Role of Au in the Growth and Nanoscale Optical Properties of ZnO Nanowires. *J. Phys. Chem. Lett.* **2011,** 2 (6), 586-591.

37. Hu, J. Q.; Li, Q.; Meng, X. M.; Lee, C. S.; Lee, S. T., Thermal reduction route to the fabrication of coaxial Zn/ZnO nanocables and ZnO nanotubes. *Chem. Mater.* **2003,** 15 (1), 305-308.

38. Lyu, S. C.; Zhang, Y.; Lee, C. J.; Ruh, H.; Lee, H. J., Low-temperature growth of ZnO nanowire array by a simple physical vapor-deposition method. *Chem. Mater.* **2003,** 15 (17), 3294-3299.

39. Li, Q. C.; Kumar, V.; Li, Y.; Zhang, H. T.; Marks, T. J.; Chang, R. P. H., Fabrication of ZnO nanorods and nanotubes in aqueous solutions. *Chem. Mater.* **2005,** 17 (5), 1001-1006.

40. Kuo, T. J.; Lin, C. N.; Kuo, C. L.; Huang, M. H., Growth of ultralong ZnO nanowires on silicon substrates by vapor transport and their use as recyclable photocatalysts. *Chem. Mater.* **2007,** 19 (21), 5143-5147.

41. Elias, J.; Tena-Zaera, R.; Wang, G. Y.; Levy-Clement, C., Conversion of ZnO Nanowires into Nanotubes with Tailored Dimensions. *Chem. Mater.* **2008,** 20 (21), 6633-6637.

42. Li, C.; Hong, G. S.; Wang, P. W.; Yu, D. P.; Qi, L. M., Wet Chemical Approaches to Patterned Arrays of Well-Aligned ZnO Nanopillars Assisted by Monolayer Colloidal Crystals. *Chem. Mater.* **2009,** 21 (5), 891-897.

43. McPeak, K. M.; Becker, M. A.; Britton, N. G.; Majidi, H.; Bunker, B. A.; Baxter, J. B., In Situ X-ray Absorption Near-Edge Structure Spectroscopy of ZnO Nanowire Growth During Chemical Bath Deposition. *Chem. Mater.* **2010,** 22 (22), 6162-6170.

44. Schwarz, K. W.; Tersoff, J.; Kodambaka, S.; Chou, Y. C.; Ross, F. M., Geometrical Frustration in Nanowire Growth. *Phys. Rev. Lett.* **2011,** 107 (26), 265502.

45. Chou, Y. C.; Wen, C. Y.; Reuter, M. C.; Su, D.; Stach, E. A.; Ross, F. M., Controlling the Growth of Si/Ge Nanowires and Heterojunctions Using Silver-Gold Alloy Catalysts. *ACS Nano* **2012,** 6 (7), 6407-6415.

46. Rackauskas, S.; Nasibulin, A. G.; Jiang, H.; Tian, Y.; Statkute, G.; Shandakov, S. D.; Lipsanen, H.; Kauppinen, E. I., Mechanistic investigation of ZnO nanowire growth. *Appl. Phys. Lett.* **2009,** 95 (18), 183114.

47. Delalu, H.; Vignalou, J. R.; Elkhatib, M.; Metz, R., Kinetics and modeling of diffusion phenomena occurring during the complete oxidation of zinc powder: influence of granulometry, temperature and relative humidity of the oxidizing fluid. *Solid State Sci.* **2000,** 2 (2), 229-235.

48. Young, D., *High temperature oxidation and corrosion of metals*. Oxford: Elsevier, Oxford, 2008; Vol. 1, p 592.

49. Tomlins, G. W.; Routbort, J. L.; Mason, T. O., Zinc self-diffusion, electrical properties, and defect structure of undoped, single crystal zinc oxide. *J. Appl. Phys.* **2000,** 87 (1), 117-123.

50. Yang, Y. H.; Yang, G. W., Temperature dependence and activation energy of ZnO nanowires grown on amorphous carbon. *Chem. Phys. Lett.* **2010,** 494 (1-3), 64-68.

51. Tay, C. B.; Le, H. Q.; Chua, S. J.; Loh, K. P., Empirical model for density and length prediction of ZnO nanorods on GaN using hydrothermal synthesis. *J. Electrochem. Soc.* **2007,** 154 (9), K45-K50.

52. Barin, I., *Thermochemical data of pure substances*. Science Press: Beijing, 2003.

53. Kim, D. S.; Gosele, U.; Zacharias, M., Surface-diffusion induced growth of ZnO nanowires. *J. Cryst. Growth* **2009,** 311 (11), 3216-3219.

54. Dubrovskii, V. G.; Xu, T.; Lambert, Y.; Nys, J. P.; Grandidier, B.; Stievenard, D.; Chen, W.; Pareige, P., Narrowing the Length Distribution of Ge Nanowires. *Phys. Rev. Lett.* **2012,** 108 (10), 105501.

55. Oura, K.; Lifshits, V. G.; Saranin, A. A.; Zotov, A. V.; Katayama, M., Surface Science: An Introduction. In Springer: Berlin, 2003; p 452.

56. Kim, B. J.; Garcia, R. E.; Stach, E. A., Kinetics of Congruent Vaporization of ZnO Islands. *Phys. Rev. Lett.* **2011,** 107 (14), 146101.

57. Wander, A.; Schedin, F.; Steadman, P.; Norris, A.; McGrath, R.; Turner, T. S.; Thornton, G.; Harrison, N. M., Stability of polar oxide surfaces. *Phys. Rev. Lett.* **2001,** 86 (17), 3811-3814.

58. Zhong, M.; Sato, Y.; Kurniawan, M.; Apostoluk, A.; Masenelli, B.; Maeda, E.; Ikuhara, Y.; Delaunay, J. J., ZnO dense nanowire array on a film structure in a single crystal domain texture for optical and photoelectrochemical applications. *Nanotechnology* **2012,** 23 (49), 495602.

59. Kim, K.; Sirbuly, D. J., Enhanced output of nanostructured piezoelectric arrays via controlled matrix/transducer interfacial interactions. *Appl. Phys. Lett.* **2012,** 101 (21), 213114.

Figure for Table of Content (TOC)